Structural and Transport Properties of an SPC/E Electrolyte in a Nanopore

ARTICLE *in* THE JOURNAL OF PHYSICAL CHEMISTRY B · NOVEMBER 2004

Impact Factor: 3.3 · DOI: 10.1021/jp0465985

3 AUTHORS, INCLUDING:

Kwong-Yu Chan
The University of Hong Kong
187 PUBLICATIONS **4,076** CITATIONS

Structural and Transport Properties of an SPC/E Electrolyte in a Nanopore

Yuk Wai Tang,[†] Kwong-Yu Chan,*[,†] and István Szalai[‡]

Department of Chemistry, The University of Hong Kong, Pokfulam Road, Hong Kong S.A.R., China and Department of Physics, University of Veszprém, H-8201 Veszprém, P.O. Box 158, Hungary

Received: July 30, 2004; In Final Form: September 5, 2004

Equilibrium (EMD) and nonequilibrium molecular dynamics (NEMD) simulations were conducted to investigate the effects of confinement on the structural and transport properties of an electrolyte in a nanopore. The extended simple point charge (SPC/E) model was used to model water molecules in a 0.5 M KCl electrolyte. The cylindrical nanopore was smooth, structureless, and hydrophobic with a radius that varied from 4.75 to 15.8 Å. Changes in energies and structures were observed as the nanopore radius varied. The ion−ion, ion−water, and water−water interaction energies, the ion−ion and ion−water pair distribution functions, the density profiles of H and O atoms, and the water orientation about the vertical axis and around an ion were calculated in the simulations. Because of confinement in the radial direction in a narrow pore, there was incomplete solvation of ions, evidenced by less negative ion−water energy and less alignment of water molecules with the field of the ion. With a stronger confinement, H-bonding decreased, whereas the external field had a stronger influence on the orientation of the water molecules. Both EMD and NEMD results showed a decrease of ionic conductivity with decreasing pore radius, but there was an appreciable discrepancy between the conductivities obtained by the two methods for the cases of smaller pore diameters.

Introduction

The transport of electrolytes in a nanopore is important for the areas of high technology and molecular biology. A notable example is ion transport through the ion channel of a biological membrane. Complementing experimental investigations, the selectivity of calcium and sodium in a biological ion channel has been studied using Monte Carlo simulations.[1,2] The simulation results can been related to the cell activation and signaling in the voltage-gated calcium channels found in cell membranes.[3] The transport of ions in synthetic nanomaterials, such as carbon nanotubes and mesoporous carbons, can also control technologies such as batteries and fuel cells. Experimental studies of ionic transport in well-defined micropores and membranes were attempted earlier.[4−7] There are, however, rare reports of precise and well-controlled experiments to quantify ionic transport in well-defined nanopores.[8] Molecular dynamics simulations can often provide interim and complementary answers. For example, equilibrium molecular dynamics simulations have been applied to study ion transport in carbon nanotubes recently.[9] While technologies demand simulations of realistic models, a stepwise understanding has been gained using a simplified molecular model. In particular, how the confinement of a nanopore affects the transport of water molecules and ions can be revealed by a smooth, neutral, and structureless wall, before investigating the molecular details of wall−ion and wall−water interaction. Such an approach has been adopted by Lynden-Bell and Rasaiah,[10] who reported many important effects of confinement on the transport of ions and on the structure of water molecules described by the extended simple point charge (SPC/E) model. In a series of papers, the properties under confinement in a smooth nanopore of simpler electrolyte models (viz., restricted primitive model[11−13] (RPM) and solvent primitive model[14−16] (SPM)) have been studied. In addition to equilibrium molecular dynamics (EMD), nonequilibrium molecular dynamics (NEMD) simulations[12−16] can be applied to more accurately simulate the situation of ion transport under an external electric field. To obtain the conductivities of ions in EMD simulations, the Nernst−Eistein relationship is assumed for direct proportionality of conductivity and diffusivity. It was found, however, that transport properties of ions behave differently in a small nanopore, and the Nernst−Einstein relationship does not hold in confined situations.[14]

In this paper, we extended the previous EMD and NEMD simulations[12,14] of simple electrolyte models to include a more realistic water model (viz., the SPC/E[17] model). This model has been well accepted for studying the properties of water and electrolytes in the bulk phase[18−20] and applied recently to confined systems.[10,21] Some revealing details about the confinement effects on solvation, H-bonding, and ion transport have been given by Lynden-Bell and Rasaiah,[10] who studied infinite dilution of electrolyte with only one ion in an EMD simulation. Here, we used both EMD and NEMD simulation of 20 ions and >1000 water molecules for a 0.5 M KCl electrolyte. The effects of confinement on the structures of water, ion−water and ion−ion interactions, and transport of ions are investigated. Comparison of EMD and NEMD results are also made. Our investigations here focused on a smooth nanopore without any atomic structure, as opposed to some recent works with specific structures of a biological ion channel[22−24] or a Nafion membrane channel.[25]

Model and Computation Details

Water molecules are represented by the SPC/E model[17,18] having partial positive charges at two H atoms and a Lennard-

* Corresponding author. E-mail: hrsccky@hkucc.hku.hk. Fax: (852) 2857 1586.
[†] The University of Hong Kong.
[‡] University of Veszprém.

10.1021/jp0465985 CCC: $27.50
Published on Web 00/00/0000 PAGE EST: 9.9

TABLE 1: Molecular Parameters and Charges Used for Ions, SPC/E Water, and the Cylindrical Pore Wall[a]

particle	q/e	$(\epsilon/k)/K$	d (Å)	m (au)
K^+	+1	62.74	3.250	39.1
Cl^-	−1	62.74	3.785	35.5
O (H_2O)	−0.8476	78.21	3.169	18.0
H (H_2O)	+0.4238			
wall	0	78.21	3.169	∞

[a] The OH distance in SPC/E is 1 Å, and the HOH angle is 109.47°.

Jones (6−12) interaction centered at the negatively charged O atom. The electrolyte is KCL with the diameter and interaction energy of the ions described by a Lennard-Jones (6−12) potential. Table 1 lists the model parameters for ions and water molecules. The Lennard-Jones energy (ϵ) and diameter (d) parameters of the cross-interactions are calculated on the basis of the Lorentz−Berthelot combining rules.

The water molecules and ions are confined in a smooth, structureless cylindrical cell of radius R and length H. Periodic boundary conditions are applied along the axial direction of the pore. To maintain a similar number of particles for a fixed concentration of ions, the aspect ratio of pore length to radius varies in our simulations. For a short pore length, we are more concerned with the effect of long-range Coulombic interactions with periodic images. In the simulation, the long-range correction forces are added when the periodic boundary condition in the pore has an aspect ratio of less than ten. The long-range correction is based on the charged line method used previously in Monte Carlo simulations[1,26] but modified with an inclusion of image charges in MD simulations. The dot-and-line long-range interaction energy[27] between two charged particles i and j has the form

$$U_{ij} = \frac{q_i q_j}{4\pi\epsilon_0\epsilon_r}\cdot\left(\frac{1}{r_{ij}} + \frac{1}{\sqrt{x_{ij}^2 + y_{ij}^2 + (H + z_{ij})^2}} + \frac{1}{\sqrt{x_{ij}^2 + y_{ij}^2 + (H - z_{ij})^2}}\right) + \frac{q_i q_j}{4\pi\epsilon_0\epsilon_r}\left[\ln\left(3H/2 - z_{ij} + \sqrt{x_{ij}^2 + y_{ij}^2 + (3H/2 - z_{ij})^2}\right) + \ln\left(3H/2 + z_{ij} + \sqrt{x_{ij}^2 + y_{ij}^2 + (3H/2 + z_{ij})^2}\right)\right] \quad (1)$$

where q_i and q_j are the charges of species i and j, ϵ_0 is the permittivity in a vacuum, and ϵ_r is the relative dielectric constant set to unity. The first three terms in eq 1 represent the interaction with ion j and the point images in the adjacent upper and lower image cells. The last two terms represent the interaction with the two charge lines. The long-range forces are applied to all charged particles in the pore, including the partial charges of hydrogen and oxygen in water molecules. The KCl concentration is $c \approx 0.5$ M. Both EMD and NEMD simulations were carried at the same solvent packing fractions of $\eta_s = 0.555$, where $\eta_s = N_s\sigma_s^3\pi/(6V)$, N_s and σ_s are the number and diameter of water, and V is the total volume of the simulation cell. The geometrical parameters of the simulation runs and the number of particles are summarized in Table 2. For pores with $R \geq 3.5d$, the long-range correction of eq 1 was applied.

A soft repulsive shifted Lennard-Jones (LJ)-type wall potential is used to define the wall of the pore.[12,28,32] Because a truncated LJ potential of interaction was used between the wall and the solvent particles, the wall is hydrophobic. In Lynden-Bell and Rasaiah's work,[10] a smooth and hydrophobic wall was used as well. They argued that because of the symmetric force field inside a cylinder there is no difference in MD simulation except for the chemical potential required to fill the pore to a high density. In this study, the pores are assigned with a fixed number of molecules representing a certain concentration in the bulk. Grand canonical Monte Carlo (GCMC) simulations could be used to determine the equilibrium concentration in the bulk. Performing the simulation using a rough wall or a hydrophilic wall would be desirable. We focus, however, on the confinement effect with a simpler pore wall model.

TABLE 2: Set Up of EMD and NEMD Simulation Runs

R/d_w	R (Å)	H (Å)	V (nm^3)	no. of particles (N_s, N_+, N_-)
1.5	4.75	1052	33.19	1106, 10, 10
2.0	6.39	469.0	33.29	1110, 10, 10
2.5	7.92	263.0	33.19	1106, 10, 10
3.0	9.51	168.0	33.12	1104, 10, 10
3.5	11.1	117.3	33.29	1110, 10, 10
4.0	12.7	85.6	33.07	1102, 10, 10
5.0	15.8	52.0	33.20	1107, 10, 10

The wall is electrically neutral without any Coulombic interaction and is assumed to have the same permittivity ϵ_r as the inside of the pore. The wall−particle LJ cross parameters are calculated from the Lorentz−Berthelot combining rules. The physical volume of the soft-walled cell is not trivially defined. The literature definition[10] for the SPC/E model is used. The pore radius is located at a point where the wall potential reaches kT. In our simulations, this location is around the value of $R_p = R - 1.58$ Å, and the physical radii of all pores are calculated in this manner. The physical volume of the pore is defined as $V = \pi H R_p^2$, and the actual values in various simulated cases are listed in Table 2.

NEMD simulations are performed with the presence of an external electric field driving the movement of ions. To maintain a constant temperature, the ohmic heat generated by current passage is removed by applying a Gaussian thermostat. The corresponding equation of motion for both the translational and rotational degrees of freedom are non-Newtonian but can be solved numerically in a manner similar to the Newtonian equations. Quaternions are used for the rotation of water molecules.[29] The Verlet algorithm documented by Heyes[30] is used to integrate the translation and rotation equations of motion. Under an electric field, the ions move and generate an average current after some simulation steps. The ion concentration of the simulation cell is maintained constant by a periodic boundary condition applied in the axial direction.

All simulations are carried out at 298.15 K with a 1 fs time step. Starting from a random configuration, the initial translation and rotation velocities are chosen randomly from a Gaussian distribution. For EMD simulations carried out by setting the field strength to zero, diffusion coefficients of ions in the axial direction of the pore, D_z, are calculated by the mean-square displacement method

$$D_z = \frac{1}{2}\lim_{t\to\infty}\frac{\langle|z_i(t) - z_i(0)|^2\rangle}{t} \quad (2)$$

where the broken brackets $\langle ... \rangle$ denote the ensemble average of the mean axial displacement of each ion species. The systems equilibrate after 1 ns, and the mean-square displacement of ions is measured for a 1 ns interval using a multiple origin method with a separation of 2 ps.

In the NEMD simulations, external fields are applied along the axial direction, and the conductivity of ions is calculated

TABLE 3: Average Energies and Transport Properties of a 0.5 M KCl Solution Confined in Nanopores from EMD Simulations[a]

R (Å)	U_{ii} (kJ mol^{-1})	U_{iw} (kJ mol^{-1})	U_{ww} (kJ mol^{-1})	D_+ ($\times 10^{-10}$ m^2 s^{-1})	D_- ($\times 10^{-10}$ m^2 s^{-1})	D_w ($\times 10^{-9}$ m^2 s^{-1})
4.75	-90.7 ± 11.2	-427.6 ± 16.5	-31.8 ± 0.17	4.91 ± 0.1	3.63 ± 0.2	1.70 ± 0.02
6.39	-95.8 ± 10.6	-506.6 ± 18.4	-35.4 ± 0.19	7.32 ± 0.1	5.54 ± 0.2	1.87 ± 0.01
7.92	-137.0 ± 19.3	-464.2 ± 37.9	-37.6 ± 0.35	8.08 ± 0.2	4.33 ± 0.2	1.96 ± 0.01
9.51	-128.7 ± 17.3	-483.9 ± 34.5	-38.5 ± 0.33	8.74 ± 0.5	6.66 ± 0.3	2.17 ± 0.02
11.1	-121.3 ± 21.3	-500.1 ± 42.4	-39.1 ± 0.39	8.33 ± 0.4	8.52 ± 0.5	2.31 ± 0.02
12.7	-111.5 ± 19.4	-519.2 ± 38.4	-39.4 ± 0.37	9.31 ± 1.1	14.4 ± 0.4	2.65 ± 0.01
15.8	-113.4 ± 20.0	-514.9 ± 39.4	-40.1 ± 0.41	11.8 ± 0.8	10.4 ± 0.5	2.68 ± 0.02

[a] Diffusion coefficients in z-direction are obtained by the mean-square displacement method. (D_+ for cation, D_- for anion, and D_s for water; U_{ii} is ion−ion interaction energy per ion, U_{iw} is ion−water interaction energy per ion, and U_{ww} is water−water interaction energy per particle in the pore.)

by the current density, J_z, induced in response to the electric field, E_z

$$J_z = \frac{1}{V}\sum_{j=1}^{N_i} q_j v_{j,z} \tag{3}$$

where $v_{j,z}$ is the axial component of the velocity, q_j is the charge of jth ion, V is the physical volume of the pore, and N_i is the total number of ions. In the linear response range, the direct current (dc) electric conductivity, κ, can be defined by a simple limit as

$$\kappa = \lim_{E_z \to 0} \frac{J_z}{E_z} \tag{4}$$

Conductivities at different field strengths are extrapolated to give the zero-field conductivity of the electrolyte. Five different field strengths are applied in NEMD simulations, and they lie between 1.06×10^8 and 5.3×10^8 V m^{-1}. The data are obtained by running a 1.5 ns interval for each electric field strength.

Results and Discussion

Confinement Effect on Solvation. The effect of confinement on solvation of ions can be analyzed from the average potential energies and the structural properties as the pore diameter decreases. Table 3 lists the ion−ion, ion−water, and water−water potential energies in kilojoules per mole of ions or mole of water molecules. The ion−water interaction includes the averages of cations and anions. It represents the solvation energy of ions in the pore. The ion−water potential energy is less negative than literature results for bulk solutions[16] of −606.5 and −575.6 kJ mol^{-1} for K^+ and Cl^-, respectively. The average ion−water energy weakens steadily with decreasing pore diameter because of incomplete solvation in a narrow channel, as reported previously.[10] For the narrowest pore ($R = 4.75$ Å), the energy is −427.6 kJ mol^{-1}, about 72% of the reported value in bulk KCl solution. In a narrow pore, the water molecules are not able to solvate the ions isotropically but only in the axial direction. As a result, the configuration of solvated ions in a pore is energetically less favorable compared with the bulk electrolytes and gives a less negative interaction energy. The averaged potential energies in NEMD simulations for two of the applied fields are shown in Table 4. Between the values at the two applied fields, ion−water energy values at the high field are generally slightly less negative, but the difference is within the statistical error estimates. The NEMD ion−water energies are also in agreement with the EMD results within the statistical error estimates. The applied electric field in reduced unit is defined as the product of the electric field, the electronic charge, and the diameter of the water molecule, and divided by the LJ energy of water in Table 1.

TABLE 4: Average Energies and Transport Properties of a 0.5 M KCl Solution Confined in Nanopores from NEMD Simulations[a]

R (Å)	E_z*	J_z ($\times 10^7$ Am^{-3})	U_{ii} (kJ mol^{-1})	U_{iw} (kJ mol^{-1})	U_{ww} (kJ mol^{-1})
4.75	5	0.047 ± 1.32			
	10	0.767 ± 0.96	-58.7 ± 9.5	-460.1 ± 17.4	-32.7 ± 0.16
	15	1.31 ± 1.06			
	20	1.58 ± 0.55	-52.3 ± 18.5	-422.4 ± 38.4	-34.0 ± 0.22
	25	3.04 ± 1.15			
6.39	5	1.08 ± 0.91			
	10	2.55 ± 0.68	-88.2 ± 14.0	-508.3 ± 29.7	-35.5 ± 0.30
	15	4.13 ± 0.63			
	20	5.89 ± 0.74	-92.2 ± 23.0	-489.8 ± 36.7	-35.8 ± 0.34
	25	7.33 ± 1.34			
7.92	5	3.31 ± 1.09			
	10	6.59 ± 1.08	-113.3 ± 16.0	-505.6 ± 32.2	-37.3 ± 0.32
	15	8.71 ± 0.91			
	20	12.7 ± 1.46	-113.0 ± 12.2	-499.6 ± 24.0	-37.5 ± 0.24
	25	15.4 ± 1.46			
9.51	5	3.17 ± 1.00			
	10	8.05 ± 1.31	-116.6 ± 16.9	-504.7 ± 33.0	-38.4 ± 0.31
	15	10.4 ± 0.93			
	20	13.3 ± 1.29	-122.8 ± 15.2	-488.2 ± 29.2	-38.6 ± 0.27
	25	18.8 ± 1.71			
11.1	5	3.76 ± 0.84			
	10	8.14 ± 0.87	-112.7 ± 15.9	-514.4 ± 31.2	-39.1 ± 0.30
	15	12.2 ± 0.85			
	20	16.2 ± 1.30	-121.8 ± 16.7	-492.0 ± 32.8	-39.3 ± 0.32
	25	19.9 ± 1.94			
12.7	5	4.34 ± 1.54			
	10	8.66 ± 1.06	-104.4 ± 16.4	-530.7 ± 32.3	-39.3 ± 0.31
	15	12.7 ± 1.97			
	20	17.3 ± 1.88	-122.5 ± 15.9	-492.8 ± 31.6	-39.8 ± 0.32
	25	22.0 ± 2.68			
15.8	5	4.06 ± 1.36			
	10	9.99 ± 1.51	-110.9 ± 21.4	-518.5 ± 42.1	-40.1 ± 0.43
	15	13.9 ± 1.66			
	20	18.2 ± 2.02	-115.2 ± 26.1	-506.8 ± 50.9	-40.3 ± 0.50
	25	23.9 ± 2.10			

[a] E_z* is the applied field strength in reduced unit; J_z is the current density in amperes per cubic meter.

The effect of confinement on solvation is also apparent in the structural properties of ion and water. Figure 1 shows the radial distribution functions of hydrogen and oxygen atoms in the SPC/E model around potassium ions in EMD simulations and NEMD simulations. The functions for the two larger pores are similar to those of the bulk reported in the literature.[20] The function for the pore with $R = 4.75$ Å shows some deviation from the bulk result. The oxygen peak is lower but located closer to the K^+ ion. The lower peak represents the loss of solvation in the radial direction. It is not possible to have more than two particles in any cross section, and the ions are not completely shielded by the water molecules in the radial direction. The shift in peak indicates a tighter packing in the anisotropic narrow

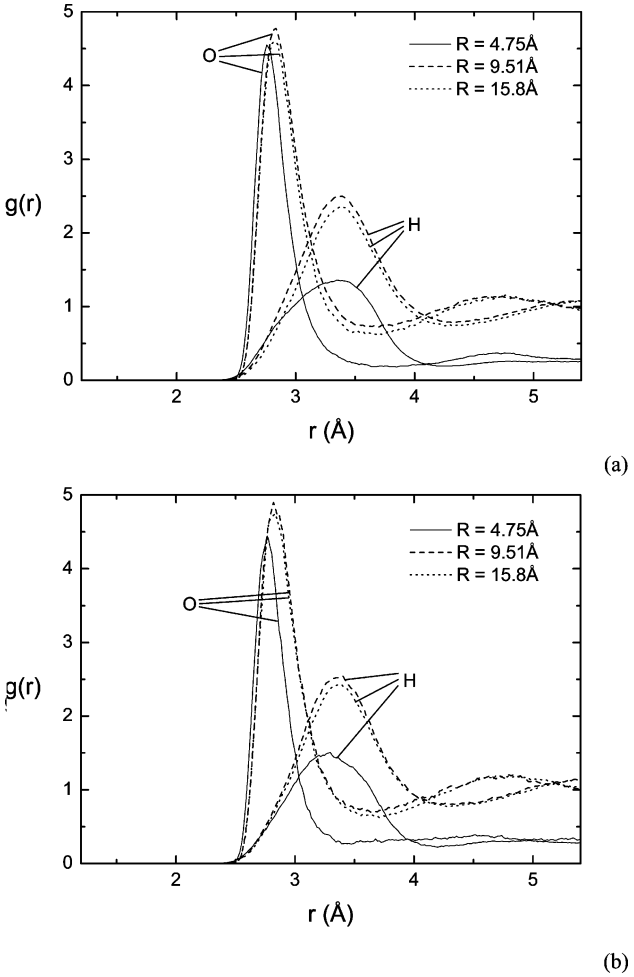

Figure 1. Radial distribution functions of oxygen (O) and hydrogen (H) atoms on SPC/E water molecules vs the distance away from a K^+ ion in (part a) EMD simulations and (part b) NEMD simulations with an applied field of $E_z^* = 20$.

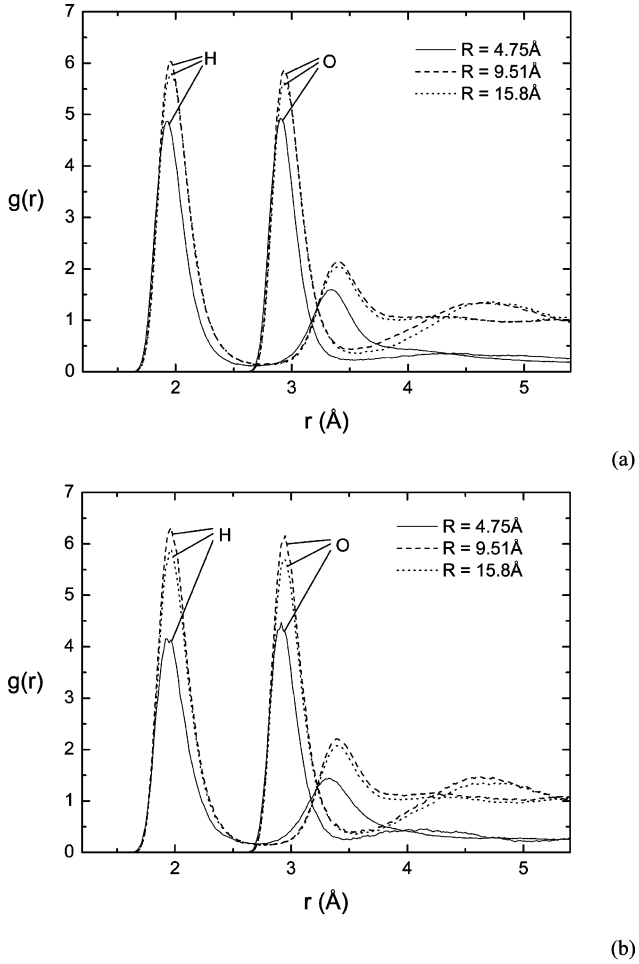

Figure 2. Radial distribution functions of oxygen (O) and hydrogen (H) atoms on SPC/E water molecules vs the distance away from a Cl^- ion in (part a) EMD simulations and (part b) NEMD simulations with an applied field of $E_z^* = 20$.

channel geometry. For the narrowest pores, the long-range value of the pair distribution is less than 1.0 because of the anisotropic geometry and the insufficient number of particles in the radial direction. No correction or renormalization has been made for this geometry factor, but the short-range and contact peaks values should be unaffected and relevant for analyses.

The pair distribution functions around chloride ions are shown in Figure 2. Two distinguishable peaks are observed for the pair correlation functions of the hydrogen atom. The first H peak of the radial distribution function, representing contact with Cl^- ion, is 1 Å from the oxygen peak. In the SPC/E model, the OH bond distance is 1.0 Å. This shows that one OH bond is almost aligned with the Cl^- radial vector. The second H peak of the radial distribution function is 0.4 Å from the oxygen peak, showing the equatorial OH position (Figure 3a). In a similar manner to the pair correlation functions around the K^+ ions in Figure 1, the profiles for the pore with $R = 4.75$ Å have lower contact peaks due to the effect of confinement on solvation. The distribution functions from the NEMD simulations are similar to those from EMD simulations, so there is no apparent effect of external field on the structure of ion and solvent particles, except for the contact peaks in the case of the smallest pore.

Solvation can also be investigated by the orientation of water near an ion. The probability distribution of angle θ between the intermolecular axis of ion and water (centered at oxygen) and the water dipole (Figure 3a) is measured for all solvent molecules located immediately around the ions in the simulation. The water dipole is defined as the vector between the two OH bonds, pointing away from the oxygen atom. The probability distribution of water dipole orientation, $P(\theta)$, is calculated as

$$P(\theta) = \frac{P_i(\theta)}{\sum_i P_i(\theta)} \tag{5}$$

where the probability for an individual angle has to be normalized by the following equation

$$P_i(\theta) = \frac{P_{u,i}(\theta)}{\sin\theta} \tag{6}$$

The range of θ is from 0° to 180°.

Figure 4 shows the probability distribution function of θ around potassium and chloride ions from both EMD and NEMD simulation results. The confinement effect is evident as the probability function of the $R = 4.75$ Å case differs from the others significantly. Around the K^+ ion, the favored angle is approximately zero with the two OH bonds evenly pointing away from K^+. For the $R = 4.75$ Å case, the peak nearby is enhanced, showing a stronger orientation alignment. As discussed earlier, there are fewer solvating water molecules, due to confinement in the radial direction. The probability angular distribution is normalized among the contacting water molecules.

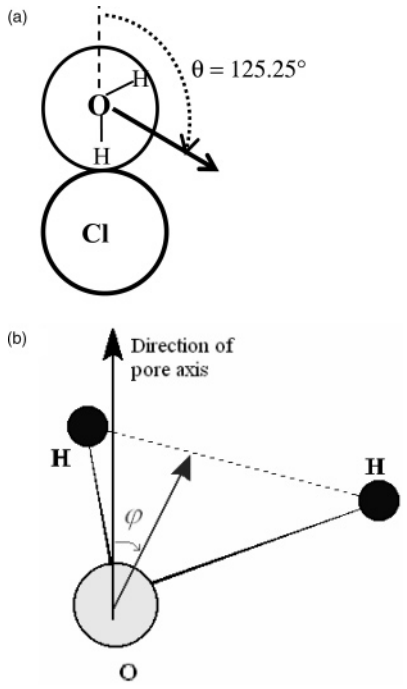

Figure 3. (part a) Definition of θ and the favored orientation of the water dipole around a Cl^- ion. (part b) Definition of the angle (φ) between the water dipole and the axis of the pore.

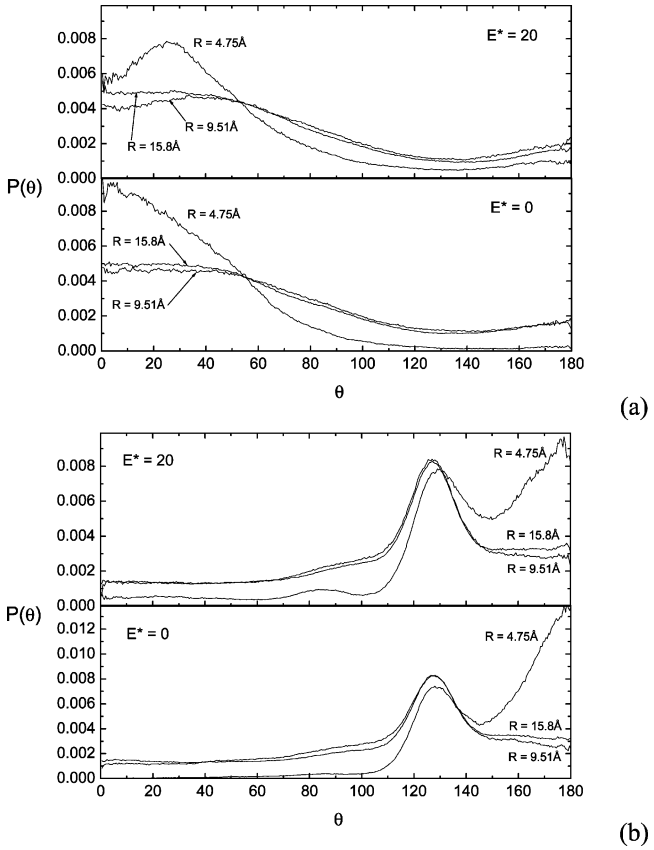

Figure 4. Probability density function of θ, the angle between the dipole of water and the radial vector from (part a) K^+ ion and (part b) Cl^- ion for three different pore diameters. The upper panel has results from NEMD simulations, while the lower panel has results from EMD simulations

The few solvating water molecules, which are vertical neighbors of the ion, and the vertical alignment should have led to the stronger orientation. Around the Cl^- ion, the probability angular distribution function has a peak at 125°, which represents the orientation in Figure 3a of the water dipole around Cl^- for the pore with $R = 4.75$ Å is different from the other models (Figure 4b). The function for $R = 4.75$ Å, however, shows an additional peak at 180° with both OH bonds close to the Cl^- ion. As will be discussed in the following section, the three-dimensional water molecule hydrogen bonding is weakened in the narrowest pore and could have attributed to a change of orientation.

The effect of the external field on the orientation of water around an ion is more apparent, but only for the case of the narrowest pore $R = 4.75$ Å. In this case, the solvating water molecules are mostly above or below the ion, assuming a vertical channel. As it is affected by the field of the ion, the orientation of the water above and below should therefore be exactly opposite. The external field should therefore distort the symmetry and favor the orientation of one group of water molecules. The molecules with the disfavored orientation would therefore tilt to compromise the competing fields of the ion and the external field. This results in a shift of the peak from 0° to about 30° in Figure 4a and the enhanced peak at 180° in Figure 4b for the case of $R = 4.75$ Å in the NEMD simulation.

H-Bonding, Structure, and Orientation of Water. Confinement also has a significant effect on the structure of water. Because the number of water molecules is more than 50 times the number of ions, except in the immediate solvation shell, the three-dimensional tetrahedral H-bonding network is the preferred low-energy structure. As observed earlier,[10] the confinement and concavity of a narrow channel prevents extension of the H-bonding network in the radial direction, and some H atoms are closer to the pore wall and free from any H-bonding. An illustration of this is given in Figure 5 for a typical snapshot of an NEMD simulation for the case of $R = 4.75$ Å. It can be seen that most of the water molecules have one H atom close to the wall that is not H-bonded, because there are no nearby oxygen atoms. From Table 3, the water−water interaction energy U_{ww} becomes less negative with a decrease of pore diameter, and the decrease is most significant in the case of the narrowest pore, $R = 4.75$ Å. This is a direct result of the disruption of the hydrogen bonding network and some H atoms near the pore wall not being H-bonded. From Table 4, the values of U_{ww} for NEMD are in close agreement with those of EMD to within the statistical error, showing no appreciable effect of external field on water−water interaction energy.

The effect of the wall on the structure of water can be studied by the density profiles of H and O atoms along the radial direction of the pore, as shown in Figure 6. Because the profiles are symmetrical about the pore axis, extended profiles across the diameter of the pore can be obtained by adding the mirror images of those shown in Figure 6. The changes of profiles with different pore diameters are due to packing of molecules in the cross-section of the channel. The results are in agreement with the literature.[10] For the pore with $R = 4.75$ Å, the physical radius is the same as the diameter of a water molecule. One density peak is observed off the central axis, and a maximum packing of two molecules is expected in the radial cross-section. For the cases of $R = 6.34$ and 9.51 Å, the pore allows packing of three and five ions, respectively, across the pore diameter, and the H and density profiles have peaks at the center of the pore. The density profile for the larger pore ($R = 15.8$ Å) does not have peaks in the core region of the pore, indicating uniform bulk solution behavior in the middle of large pores. The density functions of the H atom are twice as large, because the ratio of H/O in a water molecule is 2:1. For the first layer of water close to the wall, there are two H peaks on either side of the O

Figure 5. A snapshot of the configuration in an NEMD simulation for the case of $R = 4.75$ Å. (The large black sphere is a potassium ion. The smaller black spheres are H atoms, and the oxygen atoms are shown in gray.)

peak with a small extended region of H atoms toward the wall. This indicates the presence of H atoms closer to the wall, which are free from H-bonding. The separation of the two H atom peaks and the relative intensity of the H peak adjacent to the wall increase with decreasing pore diameter. For the case of $R = 4.75$ Å, the height of the first H peak is the same as the O peak, indicating that as much as half of the H atoms are located much closer to the pore wall than the O atoms (Figure 6). Except for the case of $R = 4.75$ Å, the effect of the external field on the distribution of H and O atoms is not apparent. In the narrowest pore of $R = 4.75$ Å, the application of the external field has led to a shift of the H peak closest to the wall toward the O peak, as shown in Figure 6a. In the same figure, the NEMD results also show a narrower H peak to the left of the O peak. These suggest a change of orientation of the water molecules with more vertical alignment in the presence of an external field. Figure 5 shows a typical NEMD configuration with many water dipoles pointing upward.

The orientation of water in different cylindrical shell layers can be further studied via the angular distribution function of

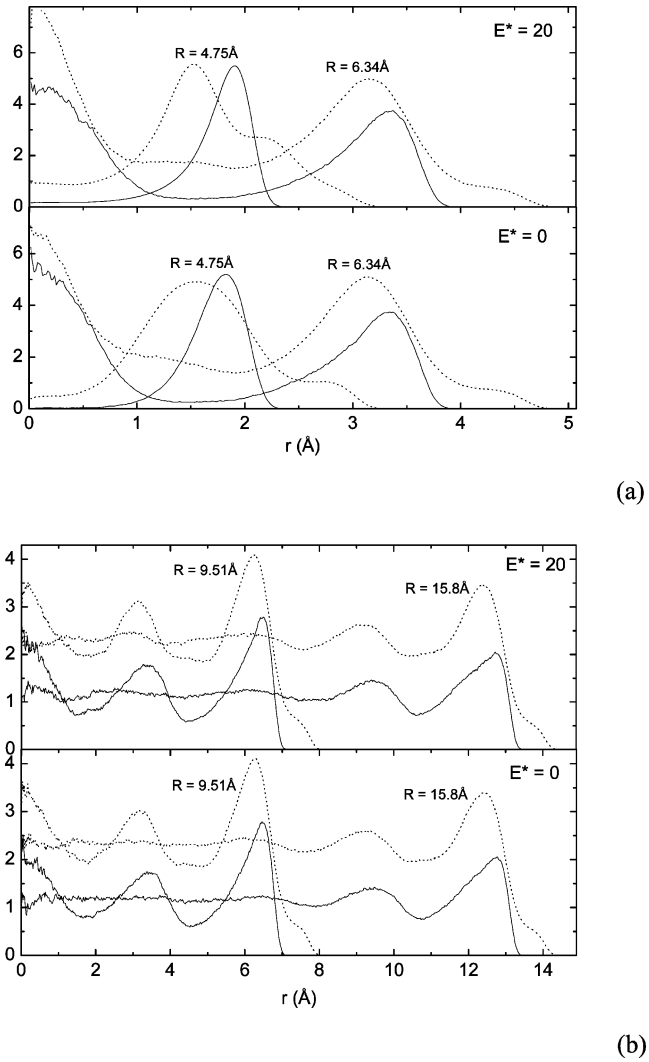

Figure 6. Density profiles of hydrogen atoms (···) and oxygen atoms (—) on water molecules in NEMD (upper panel) and EMD (lower panel) simulations.

the water dipole defined in the literature.[31] The angle between the water dipole and the vertical (parallel to pore) axis can be analyzed with the angle φ ranging from 0° to180°, as defined in Figure 3b. Probability distribution functions of the water dipole orientation are calculated in the same way as in eq 5. Each layer of water has a thickness of one molecular diameter. By comparing the angular distribution of water dipole in the layer next to the wall, it is possible to observe the effect of the wall on the orientation of the dipoles. Figure 7 shows the distribution functions of the angle, $P(\varphi)$. For the case of $R = 4.75$ Å, there is only one layer of particles next to the wall. For the case of $R = 6.39$ Å, there are two layers, one in the center and the other adjacent to the wall. For the larger pores, only the results of the first two layers next to the wall are shown, because the core layers have bulk behavior.

For water molecules in the inner layers of larger pores ($R = 9.51$ and 15.8 Å), there is no preferred orientation relative to the vertical, as the EMD angular distributions are flat (Figure 7c). This suggests random orientation of water in the core region of a larger pore, and the formation of three-dimensional H-bonding with all orientations is possible. The application of an external field, however, will distort their orientation (upper panel of Figure 7c), with the preferred orientation at 0°. The orientation of water in the layer next to the wall is different with preferred vertical up (0°) or down (180°) orientations in

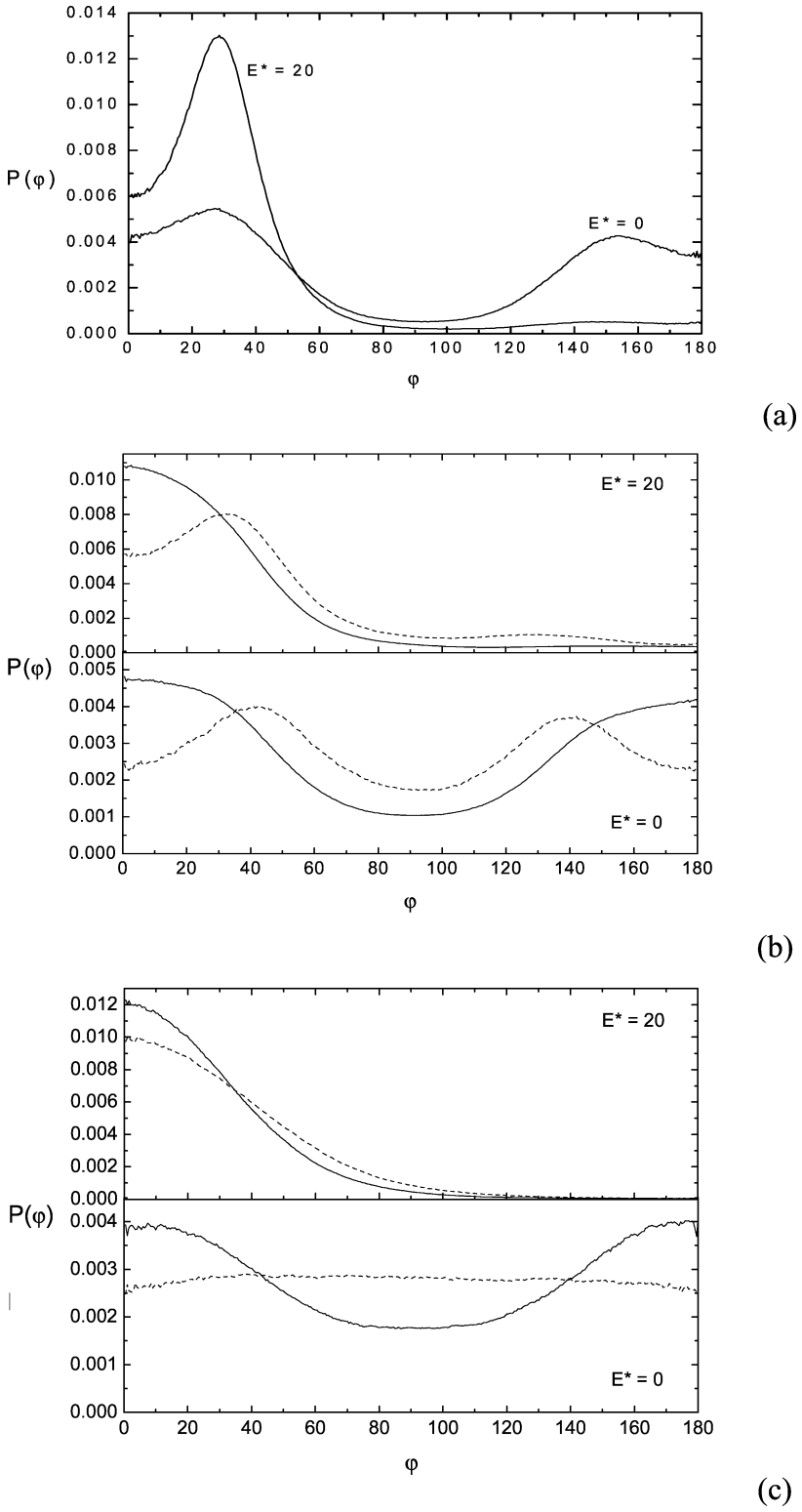

Figure 7. Probability density functions of the vertical angle, $P(\varphi)$, sustained by the water dipoles for NEMD and EMD simulations with (part a) $R = 4.75$ Å, (part b) $R = 6.39$ Å, and (part c) $R = 15.8$ Å. The solid lines (—) are the functions of the layer of molecules next to the wall, and the dashed lines (- - -) are from the next inner layers.

EMD. With the application of an external field, there is only one preferred orientation.

For the case of $R = 6.39$ Å, however, the inner layer of the pore does not have a flat angular distribution function (Figure 7b). Instead, two peaks located at approximately 40° and 140° are observed. In this case, there are three particles across the diameter of the pore, and the inner layer of the distribution function represents the particles located along the axis of pore. The 40° and 140° suggests orientations with one of the OH bonds aligning with the vertical axis, forming an H-bond with the upper or lower neighbor, whereas the other OH bond will form an H-bond with the water in the layer next to the wall. For water in the layer next to the wall, the two preferred orientations are vertical up (0°) or down (180°) orientations in

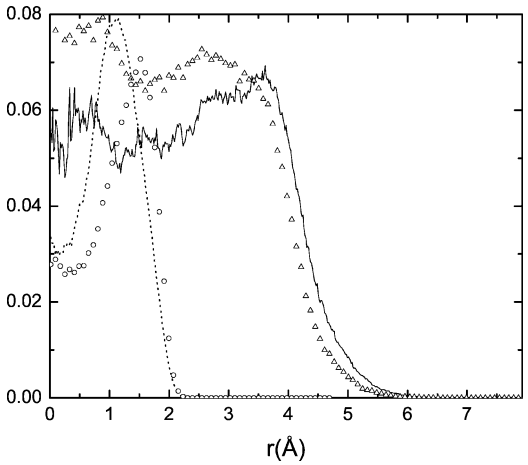

Figure 8. Density profiles of ions along the radial direction of pores with $R = 4.75$ Å, $E^* = 0$ (····), and $E^* = 20$ (○); and $R = 9.51$ Å, $E^* = 0$ (—), and $E^* = 20$ (Δ).

EMD, as in the case of larger pores. The application of an external field will flip some of the water molecules, and only one of the two orientations is preferred in both layers of water.

For the case of $R = 4.75$ Å, there is only one layer of water. The preferred orientations (30° and 150°) are like the second layer (40° and 140°) of the case of $R = 6.39$ Å. Because there are two water molecules in a cross-section in the case of $R = 4.75$ Å, the H-bonding between them will not lead to a 0° or 180° orientation. The tilt suggests H-bonding with the lower or upper neighbors. With the 30° and 150° orientation, the OH bonds that are not H-bonded will point more toward the wall, as shown in Figure 6a in the density profiles of H atoms and in Figure 5. Again, with the application of an external field, only one of the two orientations is preferred.

Confinement Effect on Ion−Ion Interaction. Because there are only 20 ions, the ion−ion potential energy values show large statistical variations up to 30%. The values of ion−ion interaction energy in EMD simulation of the 2 smaller pores ($R = 4.75$ Å and $R = 6.39$ Å) are more positive than those of larger pores. The weaker ion−ion interaction appears strange initially, because there is less solvation in the smaller pores, as discussed earlier. This weakening of ion−ion interaction can be explained by the longer average distance between ions in a smaller pore with less cross-sectional area, as discussed previously for simulations with the RPM and SPM electrolyte models.[12,14] Density profiles of ions show that the ions are more evenly distributed along the radial direction of the pore for $R = 9.51$ Å (Figure 8) compared to the case of $R = 4.75$ Å. The confinement effect induces more ion pairings, as observed in the K^+ Cl^- pair distribution functions of Figure 9 for different pore diameters. The contact peak increases from 7.5 in the case of $R = 12.7$ Å to 25 in the case of $R = 4.75$ Å. The observation of more ion pairing in a narrow pore has been reported previously by Nicholson and Quirke.[9] As shown in Figure 9, the application of an external field does not change the values of the contact peaks and the amount of ion pairing. In the case of a bulk fluid, the proportion of ion pairs can be calculated by finding the ratio of the integral of the first peak of the pair correlation function to the integral of the whole function. However, this technique is practically difficult for ions in a cylindrical pore, because the radius of the pore is usually very small, and the pair correlation function will appear truncated beyond the wall radius.

Transport Properties of Electrolytes. The dynamic properties of electrolytes are studied in both EMD and NEMD simulations. In EMD simulations, mean-square displacements of both cation and anion are measured over a period of 1 ns with the method of multiple origins[32] separated by 2 ps. Figure 10 shows the average mean-square displacements of ions over 500 time origins for pores with radii $R = 4.75$ and 9.61 Å. The mean-square displacements of K^+ are higher than that of Cl^-. The curves of mean-square displacement of ions in the narrowest pore have ripples, because ions in the narrowest pore are restricted to nearly one-dimensional motion. In the calculation of a diffusion coefficient of ions in a nanopore, the use of velocity autocorrelation gives a much higher value of the diffusion coefficient because of the short relaxation time of the function. Self-diffusion coefficients of an ion species are related to autocorrelation functions by

$$D_z = \int_0^\infty \langle v_z(t) \cdot v_z(0) \rangle \, dt \tag{7}$$

The diffusion coefficients calculated by autocorrelation functions of molecules in the narrow pores can be three times larger than those calculated by the mean-square displacement method. The

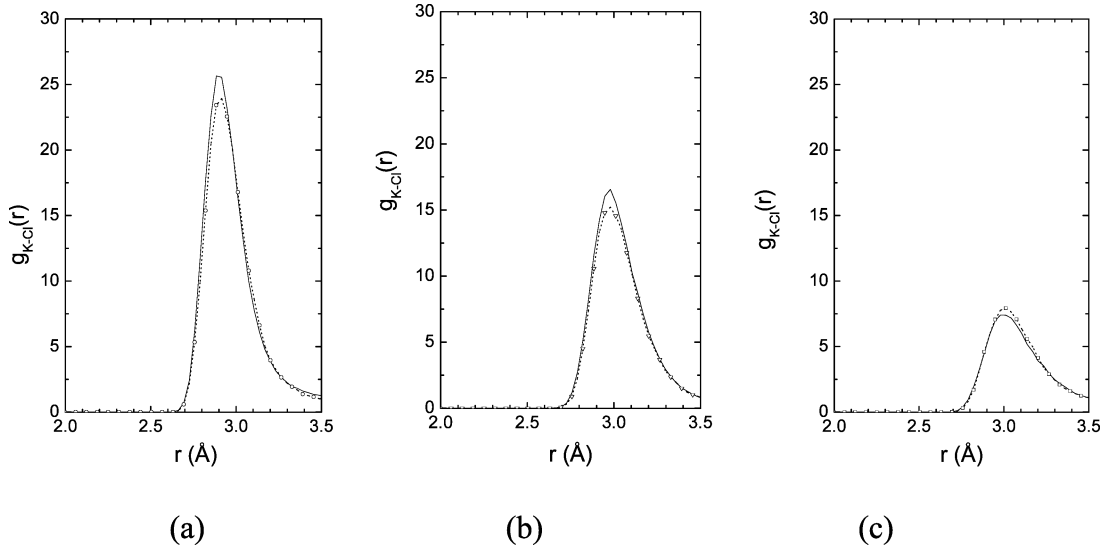

Figure 9. K^+ Cl^- pair correlation functions for pores of (part a) $R = 4.75$ Å, (part b) $R = 6.39$ Å and (part c) $R = 12.7$ Å. In each graph, the solid lines (—) are results from EMD simulations, while the dotted lines (···) with the hollow symbol are NEMD results with an applied field strength of $E^* = 20$.

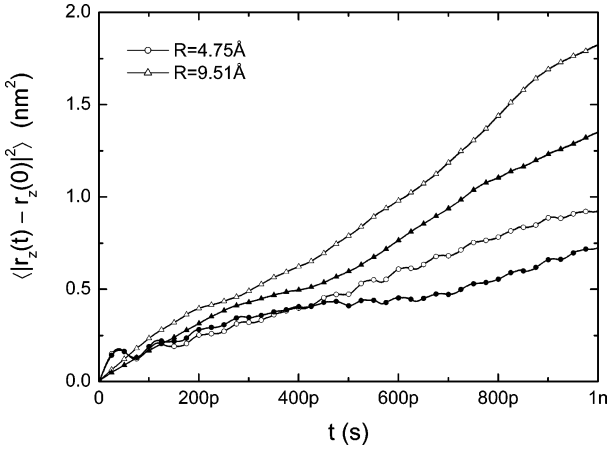

Figure 10. Mean-square displacement of K^+ (open symbols) and Cl^- (solid symbols) in pores with radii $R = 4.75$ Å and $R = 9.51$ Å.

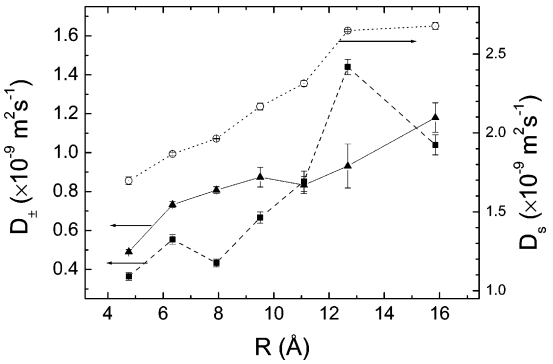

Figure 11. Self-diffusion coefficients of K^+ (▲), Cl^- (■), and H_2O (○) in nanopores of different diameters.

autocorrelation function of velocity only gives the diffusivity on a short time scale of 1 ps in our case. As shown in Figure 10, that region cannot represent the long time scale diffusivity of ions in the pore. Therefore, the results of diffusivities calculated by the autocorrelation functions are not reported.

Diffusion coefficients of K^+, Cl^-, and H_2O in a nanopore calculated by the mean-square displacement method are shown in Table 3 and Figure 11. They are determined by the data points between 500 ps and 1 ns in Figure 10, and the uncertainties of the linear fittings are shown in Table 3. Unlike the common method in which the number of time origin averages decrease with increasing time, we used the same number of time origins for all time regions. In general, diffusion coefficients of all species decreases with decreasing pore diameter because of the confinement effect of nanopores. When the pore radius is less than 10 Å, diffusion coefficients of Cl^- ions are more than 25% less than those of K^+. The confinement effect on anions is more severe, because the size of anions is larger. The diffusivity of water levels off at $\sim 2.7 \times 10^{-9}$ m^2 s^{-1} for $R > 12.7$ Å. This value is close to the corresponding value in bulk solution.[20] The confinement effect is less significant for water in large pores. Though there is less solvation of ions due to confinement, there is an increase in ion pairing, as discussed earlier. This may have contributed to the decrease in mobility of individual ions.

Current densities of ions at different field strengths in the NEMD are calculated, and the values are shown in Table 4. The results are the averages of simulation over a period of 1 ns. The error bars are the standard deviation of current densities and are larger for results in small pores and small fields, particularly for the result of $E^* = 5$ and $R = 4.75$, 6.39 Å. The simulation of each pore diameter is performed with five different field strengths to obtain better results for the zero-field

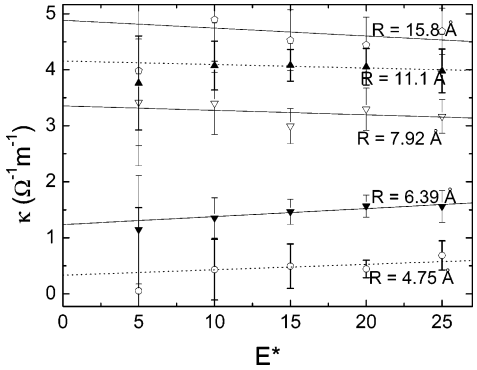

Figure 12. Conductivity of SPC/E model electrolyte as a function of reduced electric field strength for different pore diameters.

TABLE 5: Comparison of Transport Properties of a 0.5 M KCl SPC/E Electrolyte Confined in Nanopores by EMD and NEMD Simulations[a]

R (Å)	κ (EMD)	κ (NEMD)
4.75	1.60 ± 0.06	0.334 ± 0.11
6.39	2.41 ± 0.07	1.22 ± 0.47
7.92	2.33 ± 0.07	3.45 ± 0.18
9.51	2.90 ± 0.15	3.44 ± 0.67
11.1	3.15 ± 0.18	4.06 ± 0.56
12.7	4.47 ± 0.29	4.27 ± 0.06
15.8	4.17 ± 0.24	4.90 ± 0.36

[a] Electrical conductivity is expressed in units of Ω^{-1} m^{-1}.

conductivities. Because of the large deviation, the above two data points are excluded in the calculation of zero-field conductivities. The effect of confinement is particularly strong for the pore with $R = 4.75$ Å when the pore is just large enough for two ions to pass each other. Field-dependent conductivities of ions are shown in Figure 12. Conductivities of ions for each pore size have a linear relationship with electric field strength, albeit with some scattering. Ionic conductivity drops significantly for electrolytes inside pores with $R < 7.92$ Å, which indicates a stronger confinement effect from the wall of the cylindrical pore.

Zero-field conductivities (κ) of electrolytes obtained in NEMD simulations by the extrapolation in Figure 12 are listed in Table 5. For comparison, the electrical conductivity is estimated from the diffusion coefficients obtained in EMD simulations by the Nernst−Einstein relation. For a univalent 1:1 KCl solution, the relationship is

$$\kappa = \frac{e^2}{kT}(D_+\rho_+ + D_-\rho_-) \tag{8}$$

where e is the elementary charge, D_+ and D_- are the diffusion coefficients of K^+ and Cl^-, and ρ_+ and ρ_- are the densities of K^+ and Cl^-, respectively. Conductivities in different pores estimated from EMD are also shown in Table 5, and the values are compared against the NEMD results in Figure 13. Conductivity obtained by EMD increases more gradually with pore radius, while conductivity obtained by NEMD increases sharply from $R = 4.75$ to 7.92 Å before leveling off. The confinement leads to an increase of ion pairing, which will move more slowly compared to individual ions.

Conductivities of the largest pore studied ($R = 15.8$ Å) by both EMD and NEMD methods are about 18% lower than the experimental value of 5.5 Ω^{-1} m^{-1} for a 0.1 M KCl solution.[33] The discrepancy may due to some presence of the confinement effect even for the largest pore studied. The discrepancy may also come from the shortcomings in the SPC/E electrolyte model

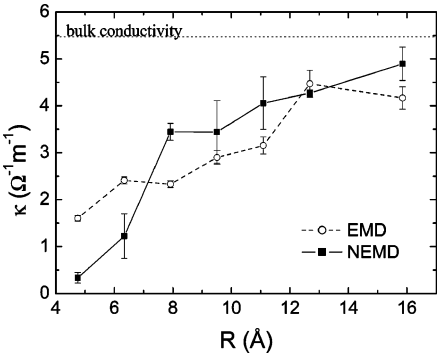

Figure 13. Comparison of ionic conductivity in the SPC/E electrolyte calculated by EMD (○) and NEMD (■) simulations. The dashed horizontal line (- - -) is the estimated experimental value of conductivity of a 0.5 M KCl bulk solution.

representing real electrolytes. For pores with $R > 6.39$ Å, conductivities found by NEMD are higher than those by EMD for most pores. From the distribution of orientation of the water dipole in Figure 9 and a typical configuration shown Figure 5, the water dipoles are pointing in one direction when an external field is applied. The regular pattern of molecules may lead to a faster diffusion of the ions inside the pore. The electrical conductivity in the pores with $R \leq 6.39$ Å found by NEMD simulations is much smaller than the EMD values. The K^+ Cl^- pair correlation functions (Figure 9) show an increase of ion pairing in the narrow pores. Under an external field in NEMD, the mobility of the ion pair may be more strongly hindered compared to EMD, because a direct current requires passage of oppositely charged ions around each other in the narrow pore.

Previous comparisons of EMD and NEMD results for simpler molecular models[5,7] have shown differences in conductivities estimated by the two methods, and the Nernst−Einstein equation does not hold for the pores with pore radius smaller than three times the diameter of ions. The results here for the SPC/E model electrolyte also show differences between the NEMD and EMD conductivities for narrow pores. The use of EMD simulations and the assumption of the Nernst−Einstein relationship may not be a suitable way to calculate electrical conductivity of electrolytes confined in a small nanopore.

In this work, a smooth and hydrophobic wall is used for a simple model to study the confinement effect. One may argue that the wall potential is not realistic, and simulations using structured pore walls can more accurately reflect a realistic situation. Nevertheless, the results here offer a clear view of the confinement effect, and further models of pore structures can provide details that are more relevant to the experimental phenomenon of electrolyte transport in a nanopore.

Summary

We have performed both EMD and NEMD simulations for a 0.5 M KCl electrolyte confined in cylindrical pores of radii 4.75−15.8 Å with water represented by the extended simple point charge (SPC/E) model. The results show a decrease in hydration of the ions and the H-bonding of water as the pore radius decreases. In addition, there is a tendency of ions to pair up in very narrow channels. The diffusion coefficients of electrolytes determined from mean-square displacements in EMD simulations and the ionic conductivity calculated in NEMD simulations decrease with decreasing pore radius. Some differences between the conductivities obtained in EMD and NEMD, however, challenge the validity of the Nernst−Einstein equation for electrolytes confined in a nanopore.

Acknowledgment. This study is supported by a grant from the Hong Kong Research Grants Council (HKU7213/99P).

References and Notes

(1) Boda, D.; Busath, D. D.; Henderson, D.; Sokolowski, S. *J. Chem. Phys. B* **2000**, *104*, 8903.
(2) Boda, D.; Henderson, D. *J. Phys.: Condens. Matter* **2002**, *14*, 9485.
(3) Hille, B. *Ionic Channels of Excitable Membranes*; Sinauer Associates: Sunderland, MA, 1992.
(4) Steck, A.; Yeager, H. L. *J. Electrochem. Soc.* **1983**, *130*, 1297.
(5) Gavach, C.; Pamboutzoglou, G.; Nedyalkov, M.; Poucelly, G. *J. Membr. Sci.* **1989**, *45*, 37.
(6) Westermann-Clark, G. B.; Anderson, J. L. *J. Electrochem. Soc.* **1983**, *130*, 839.
(7) Hansma, P. K.; Drake, B.; Marti, O.; Gould, S. A. C.; Prater, C. B. *Science* **1989**, *243*, 641.
(8) Nishizawa, M.; Menon, V. P.; Martin, C. R. *Science* **1995**, *268* (5211), 700.
(9) Nicholson, D.; Quirke, N. *Mol. Simul.* **2003**, *29* (4), 287.
(10) Lynden-Bell, R. M.; Rasaiah, J. C. *J. Chem. Phys.* **1996**, *105*, 9266.
(11) Lo, W. Y.; Chan, K. Y.; Lee, M.; Mok, K. L. *J. Electroanal. Chem.* **1998**, *450*, 265.
(12) Tang, Y. W.; Szalai, I.; Chan, K. Y. *Mol. Phys.* **2001**, *99*, 309.
(13) Tang, Y. W.; Szalai, I.; Chan, K. Y. *Mol. Phys.* **2002**, *100*, 1497.
(14) Tang, Y. W.; Szalai, I.; Chan, K. Y. *J. Phys. Chem. A* **2001**, *105*, 9616.
(15) Chan, K. Y.; Tang, Y. W.; Szalai, I. *Mol. Simul.* **2004**, *30*, 81.
(16) Lai, S. K.; Kau, C. Y.; Tang, Y. W.; Chan, K. Y. *Phys. Rev. E* **2004**, *69*, 051203.
(17) Berendsen, H. J. C.; Grigera, J. R.; Straatsma, T. P. *J. Chem. Phys.* **1987**, *91*, 6269.
(18) Van Der Spoel, D.; Van Maaren, P. J.; Berendsen, H. J. C. *J. Chem. Phys.* **1998**, *108*, 10220.
(19) Jedlovszky, P.; Richard, J. *J. Chem. Phys.* **1999**, *110*, 8019.
(20) Lee, S. H.; Rasaiah, J. C. *J. Phys. Chem.* **1996**, *100*, 1420.
(21) Crozier, P. S.; Rowley, R. L.; Holladay, N. B.; Henderson, D.; Busath, D. D. *Phys. Rev. Lett.* **2001**, *86*, 2467.
(22) Crozier, P. S.; Henderson, D.; Rowley, R. L.; Busath, D. D. *Biophys. J.* **2001**, *81* (6), 3077.
(23) Chung, S. H.; Allen, T. W.; Kuycak, S. *Biophys. J.* **2003**, *83* (1), 263.
(24) Roux, B.; Allen, T.; Bernechem S.; Im, W. *Q. Rev. Biophys.* **2004**, *37* (1), 15.
(25) Spohr, E. *Mol. Simul.* **2004**, *30*, 107.
(26) Murthy, C. S.; Bacquet, R. J.; Rossky, P. J. *J. Phys. Chem.* **1985**, *89*, 701.
(27) Tang, Y. W.; Chan, K. Y. *Mol. Simul.* **2004**, *30*, 63.
(28) Tjatjopoulos, G. J.; Feke, D. L.; Mann, A. *J. Chem. Phys.* **1988**, *92*, 4006.
(29) Allen, M. P.; Tildesley, D. J. *Computer Simulation of Liquids*; Clarendon Press: Oxford, 1987.
(30) Heyes, D. M. *Phys. Rev. B* **1988**, *37*, 5677.
(31) Shelley, J. C.; Patey, G. N. *Mol. Phys.* **1996**, *88*, 385.
(32) Frenkel, D.; Smit, B. *Understanding Molecular Simulation: From Algorithms to Applications*; Academic Press: San Diego, 1996.
(33) *CRC Handbook of Chemistry and Physics*, 3rd Electronic Edition; Knovel (http://www.knovel.com).